

# Correlative Electrochemical Microscopy for the Elucidation of the Local Ionic and Electronic Properties of the Solid Electrolyte Interphase in Li-Ion Batteries

Carla S. Santos, Alexander Botz, Aliaksandr S. Bandarenka, Edgar Ventosa,\* and Wolfgang Schuhmann\*

**Abstract:** The solid-electrolyte interphase (SEI) plays a key role in the stability of lithium-ion batteries as the SEI prevents the continuous degradation of the electrolyte at the anode. The SEI acts as an insulating layer for electron transfer, still allowing the ionic flux through the layer. We combine the feedback and multi-frequency alternating-current modes of scanning electrochemical microscopy (SECM) for the first time to assess quantitatively the local electronic and ionic properties of the SEI varying the SEI formation conditions and the used electrolytes in the field of Li-ion batteries (LIB). Correlations between the electronic and ionic properties of the resulting SEI on a model Cu electrode demonstrates the unique feasibility of the proposed strategy to provide the two essential properties of an SEI: ionic and electronic conductivity in dependence on the formation conditions, which is anticipated to exhibit a significant impact on the field of LIBs.

## Introduction

Although a Li-ion battery consists of simply three elements, i.e., positive electrode, electrolyte solution, and negative electrode, it is far from being a simple electrochemical

device. Many electrochemical processes take place simultaneously. A detailed and unambiguous investigation of the individual reactions and components remains challenging. Hence, the battery community has devoted substantial effort to developing and adapting advanced characterization techniques, which help put together all pieces of the scientific puzzle. Without an in-depth understanding of the individual elements of the contribution of each element of the complex system, sufficiently fast progress in battery research at the cell level cannot be achieved. In general, efforts have been focused on the development of two groups of techniques. In situ and operando techniques are of vital importance since information is obtained under relevant conditions, as close as possible to operating circumstances.<sup>[1,2]</sup> Moreover, spatially resolved techniques are the basis for evaluating the local heterogeneity providing access to a high number of statistically significant measurements instead of assessing the average response of the ensemble.<sup>[3,4]</sup> Several characterization methods have been developed and optimized over the last years to gain access to the correlation between chemistry, structure, morphology, and battery performance. In-depth understanding of the behavior during the charging/discharging processes can be achieved by means of micro/nanoscale analysis: for example in situ optical techniques such as Fourier Transform Infrared Spectroscopy, Raman microscopy, and X-ray-based methods were primarily explored to characterize the chemical and structural properties of the battery electrodes.<sup>[1,5]</sup> Powerful complementary tools for exploring the intrinsic physicochemical properties with high lateral resolution are scanning probe microscopy methods.<sup>[4,6]</sup> Recently, advantages of zooming-in to small subsections of the investigated battery surface have been discussed, leading to efforts to explore high-resolution electrochemical techniques and ultimately to provide access to the relation between the intrinsic characteristics of battery materials during operation.<sup>[7,8]</sup> Indeed, extremely sensitive analytical methods providing high lateral resolution are of high interest to investigate the heterogeneity of a battery electrode. In this regard, scanning electrochemical microscopy (SECM)<sup>[9,10–12]</sup> provides local electrochemical information about an operating electrode surface with a lateral resolution in the range of  $\mu\text{m}$  or even sub- $\mu\text{m}$ . SECM is a mature technique with a variety of modes of operation, which was already successfully applied for the investigation of Li-ion battery materials.<sup>[8,12]</sup> The feedback mode (FB-SECM) was employed to investigate

[\*] Dr. C. S. Santos, Dr. A. Botz, Prof. Dr. W. Schuhmann  
Analytical Chemistry—Center for Electrochemical Sciences (CES),  
Faculty of Chemistry and Biochemistry, Ruhr-Universität Bochum  
Universitätsstr.150, 44780 Bochum (Germany)  
E-mail: wolfgang.schuhmann@rub.de

Prof. Dr. A. S. Bandarenka  
Physics of Energy Conversion and Storage, Physik-Department,  
Technische Universität München  
James-Frank-Strasse 1, 85748 Garching (Germany)

Prof. Dr. E. Ventosa  
Department of Chemistry, University of Burgos  
Pza. Misael Bañuelos s/n, 09001 Burgos (Spain)  
E-mail: eventosa@ubu.es

© 2022 The Authors. Angewandte Chemie International Edition published by Wiley-VCH GmbH. This is an open access article under the terms of the Creative Commons Attribution Non-Commercial NoDerivs License, which permits use and distribution in any medium, provided the original work is properly cited, the use is non-commercial and no modifications or adaptations are made.

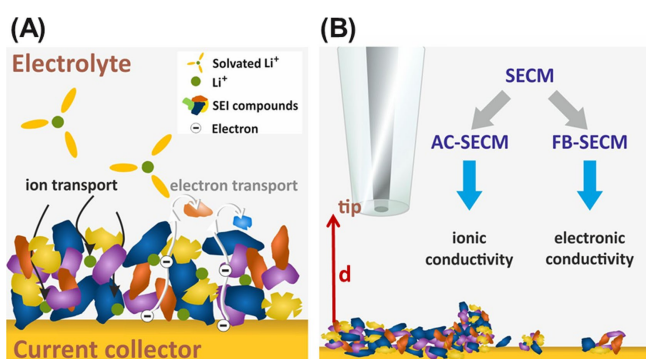
essential processes of Li-ion batteries performance,<sup>[13–15]</sup> such as key indicators of Li-ion batteries like the state of health, which is to a large extent determined by the properties of the solid electrolyte interphase (SEI) formed on the surface of the negative electrode.<sup>[16]</sup> The quality and properties of the SEI play an essential role in the battery performance and prevents continuous decomposition of the electrolyte. Therefore, the SEI has to be electronically insulating, while it needs to allow transport of desolvated Li-ions towards the active materials, as schematically shown in Scheme 1A. Although many techniques provide relevant in situ information regarding the chemical composition and morphology of the SEI, there is no technique that provides correlative microscopic information on both ionic and electronic conductivity of the SEI, which is of critical importance for the development of high-performance batteries. Ionic properties of the SEI on a macroscopic level can be assessed using electrochemical impedance spectroscopy (EIS). Moreover, in the alternating current mode of SECM (AC-SECM) was developed to locally register impedance spectra.<sup>[17]</sup> AC-SECM images are typically obtained at one pre-selected perturbation frequency to shorten the overall experimental time, and AC-SECM was mainly employed to characterize oxide films and to follow corrosion processes.<sup>[18–20]</sup> AC-SECM at multiple frequencies was proposed<sup>[21,22]</sup> but not yet applied in battery research. Despite FB-SECM was previously used together with one-frequency AC-SECM for aqueous Li-ion battery electrodes, no clear conclusion could be obtained about the SEI properties.<sup>[23]</sup> Moreover, no correlative information about electronic and ionic properties of the SEI could be derived due to the specific properties of the used battery material. A methodology to provide spatially resolved quantitative information about electronic and ionic conductivity of the SEI was not yet demonstrated. Herein, we establish and validate a correlative in situ methodology (Scheme 1B) that combines FB-SECM and multi-frequency AC-SECM for elucidating in situ and locally resolved information of the ionic and electronic properties of the SEI at identical locations both qualitatively and quantitatively. The acquisition of complete local electrochemical impedance spectra provides essential information at different frequencies and hence allows to separate the

contribution of the SECM tip from that of the SEI-modified sample surface. The deconvolution of the SECM tip contribution is crucial for separating the impact of the properties of the sample surface, demonstrating the advantage of the multi-frequency AC SECM measurement. Furthermore, the combination of both SECM techniques provides information about the role of the SEI formation protocols and the electrolyte composition on the properties of the resulting SEI.

## Results and Discussion

Considering the complexity of the multiple reactions in a porous battery electrode and the multiple parameters impacting on the battery properties, a model electrode was initially used in our work to facilitate the unambiguous interpretation of the obtained results and validation of the proposed methodology. A Cu plate typically used as the current collector serves as model electrode, since Cu metal is electrochemically inactive in the potential window in which the negative electrode usually operates (0.0–3.0 V vs. Li|Li<sup>+</sup>), is smooth and does not react spontaneously with the electrolyte. We used the Cu surface on which two well-defined regions, namely i) an SEI-covered region and ii) an SEI-free region, are generated (Figure 1A). The bare Cu plate is employed as working electrode (WE) in an open electrochemical cell on which the SEI is formed. The SEI formation was performed by scanning the potential from OCP vs reference electrode (RE) to a cut-off potential of e.g. 0 V (all potentials are referred against Li|Li<sup>+</sup> in 1 M Li<sup>+</sup>), at a scan rate of 1 mVs<sup>-1</sup> to allow decomposition of the electrolyte and formation of a thin SEI. The slow scan rate was employed to ensure uniform decomposition of the electrolyte on the Cu surface. Afterwards, the potential was held at the cut-off potential to promote thickening of the SEI for either 12 h (long-term protocol, i) or 1 h (short-term protocol, ii). The short-term protocol was also employed as an accelerated test to evaluate the influence of parameters such as electrolyte composition and current collector material on the SEI properties. A more detailed description of the model sample surfaces and SEI formation procedures is reported in section S-3 (Supporting Information) as well as in Table 1.

The feedback mode of scanning electrochemical microscopy (FB-SECM) was employed to explore the ability of the SEI to block electron transfer at the electrode surface. An essential role of the SEI on the anode is to prevent the continuous decomposition of the electrolyte during the lifetime of the battery. Thus, the initial formation of an effective and homogeneous SEI over the anode surface is of key importance to ensure a long cycle life of a LIB since a potential accumulation of even small electrolyte decomposition upon cycling leads ultimately to an irreversible loss in the energy storage capacity of the battery, e.g. 99.95 % coulombic efficiency leads to a decrease of 25 % in capacity after 500 cycles. Figure 1A shows a scheme of the electrochemical cell and a magnification of the model battery sample with the two distinct SEI-free and SEI-covered



**Scheme 1.** A) Schematic of the mass transport through the SEI at the anode. B) Illustration of two correlative SECM modes to elucidate the interfacial properties of the SEI with spatial resolution.

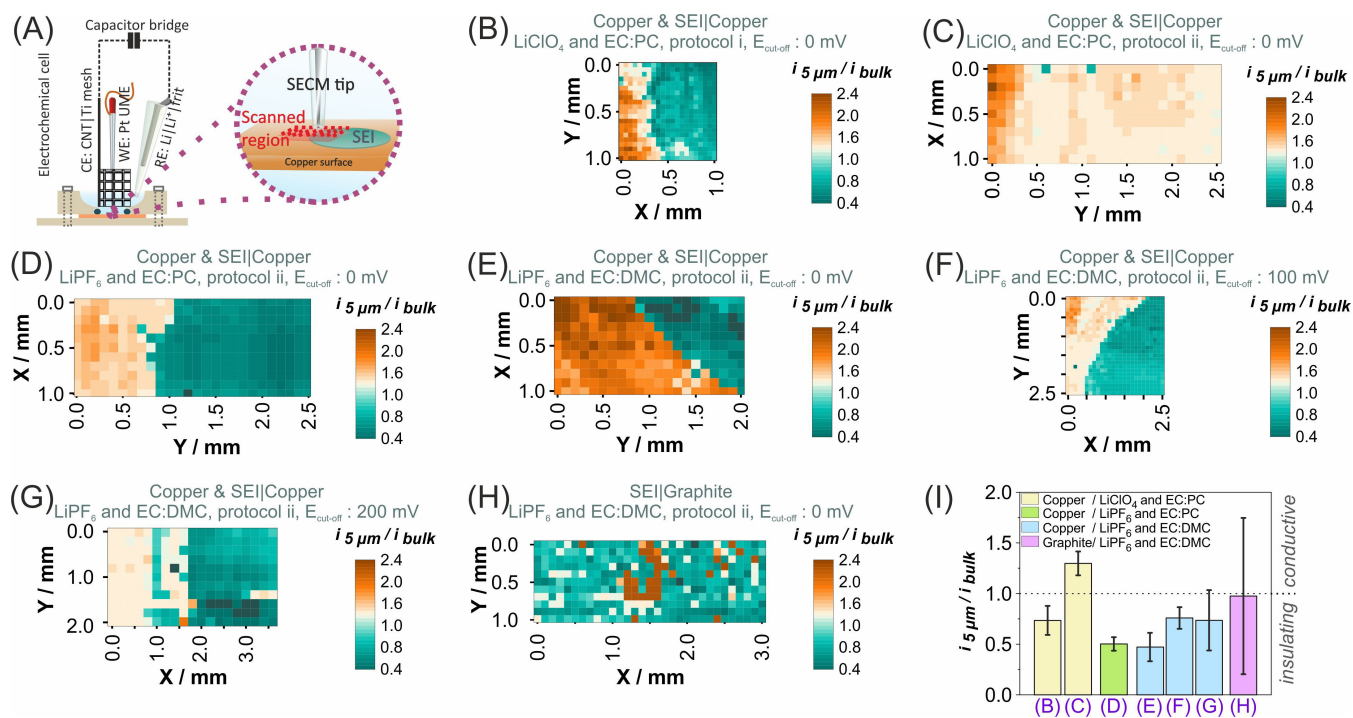


**Figure 1.** A) Schematic representation of the coaxial electrochemical cell. CE: counter electrode; WE: working electrode; RE: reference electrode. Zoom: Scheme of the scanned area in the SECM image with both the bare Cu (SEI-free) and the SEI-covered Cu area. Non-interpolated SECM images (B)–(H) of the scanned area covering the SEI-free (left) and SEI-covered (right) areas formed using the parameters as specified in Table 1. Image with a lateral pixel size in *x*- and *y*-direction of 100  $\mu\text{m}$ . Measurements were recorded in 10 mM Fc + 1 M  $\text{LiClO}_4$  and EC:PC (50/50 wt %) solution. I) Average and standard deviation of normalized local FB-SECM currents over the SEI at each SECM images of the panels (B)–(H).  $E_{\text{tip}}$ : 3.5 V vs. RE.

**Table 1:** Summary of experimental parameters during the SEI formation procedure and their corresponding figures.

Data plots	Current collector	Electrolyte composition for SEI formation procedure	Potential program for the SEI formation procedure	Cut-off potential during SEI formation [mV]
(B)	Copper	1 M $\text{LiClO}_4$ and EC:PC (50/50 wt %)	Long-term, Protocol i	0
(C)	Copper	1 M $\text{LiClO}_4$ and EC:PC (50/50 wt %)	Short-term, protocol ii	0
(D)	Copper	1 M $\text{LiPF}_6$ in EC:PC (50/50 wt %)	Short-term, protocol ii	0
(E)	Copper	1 M $\text{LiPF}_6$ in EC:DMC (50/50 v/v)	Short-term, protocol ii	0
(F)	Copper	1 M $\text{LiPF}_6$ in EC: DMC (50/50 v/v)	Short-term, protocol ii	100
(G)	Copper	1 M $\text{LiPF}_6$ in EC: DMC (50/50 v/v)	Short-term, protocol ii	200
(H)	Graphite	1 M $\text{LiPF}_6$ in EC: DMC (50/50 v/v)	Short-term, protocol ii	0

regions, respectively, of the region scanned with the SECM. Areas with sizes of 1–6  $\text{mm}^2$  were selected for SECM imaging on both the bare Cu current collector and the area modified with the SEI. The reasons to show also the bare Cu surface were to highlight the high lateral homogeneity of the bare surface but even more importantly to provide a clear visual difference between this control and the SEI-covered surface. Figure 1 shows the SECM images recorded on samples prepared with different SEI formation parameters (details in Table 1). FB-SECM experiments were performed in EC:PC (50/50 wt %) containing 10 mM ferrocene (Fc) and 1 M  $\text{LiClO}_4$ . The solvent composition for SECM imaging was chosen to prevent electrolyte evaporation during the comparatively long measurement. A self-referencing method was established for the FB-SECM measurements to diminish the effect of tip fouling and

variation of the tip response during long-term measurements (more details in Section S-5, Supporting Information).

The obtained SECM images revealed a clear difference between the bare Cu and the SEI-covered regions concerning the electronic properties. On the left side in the SECM maps, over the SEI-free region, the normalized tip current is higher than 1 (positive feedback<sup>[24,25]</sup>), which is expected for a bare metal surface. In contrast, on the right side, over the SEI-covered region, the normalized current is below 1 (negative feedback<sup>[24,25]</sup>). FB-SECM was used earlier to demonstrate the blocking properties of the SEI for electron transfer processes, evidenced unequivocally by the transition from positive feedback to negative feedback over the SEI-modified region.<sup>[10,11,13,15,26,27]</sup> The clear variation between positive and negative feedback was not noticed in the SECM image of the sample prepared with the short-term

protocol when using 1 M LiClO<sub>4</sub> in EC:PC electrolyte (Figure 1C) for SEI formation. The normalized tip current was slightly higher than 1.0 indicating that the resulting SEI poorly prevented electron transfer with the Cu surface. In contrast, the long-term SEI formation protocol clearly led to the formation of an effective SEI for this electrolyte composition, as revealed by the clear FB-SECM contrast (Figure 1B). Clearly, an electronically insulating SEI requires the long-term SEI formation protocol in 1.0 M LiClO<sub>4</sub> and EC:PC (50/50 wt %). As the SECM tip response is influenced by the vertical distance to the sample, we used an atomic force microscope (AFM) inside the glovebox to determine the thickness of the formed SEI. However, the roughness of the bare Cu surface exceeded 200 nm (Figure S3), which impeded the thickness determination of a nanolayer on top of it (expected tens of nm<sup>[28]</sup>). At the range of the determined roughness, the tip response is not significantly altered by topographic features in the SECM images with the used working distance ( $d=5\ \mu\text{m}$ ) and the SECM tip size (radius = 12  $\mu\text{m}$ ). The FB-SECM images also indicated that the formed SEI covering the Cu surface exhibited a certain level of heterogeneity, especially in the SECM image of the SEI formed following the long-term protocol in 1.0 M LiClO<sub>4</sub> and EC: PC (50/50 wt %) which coincides with previous findings concerning inhomogeneities at the protecting surface of nascent SEIs.<sup>[27]</sup> A spot with positive feedback is visible in the SEI-covered region (Figure 1B) formed following the long-term protocol in 1.0 M LiClO<sub>4</sub> and EC: PC (50/50 wt %), which suggests that the SEI properties are governed predominantly by the electrolyte composition which can only be partially mitigated by simply extending the SEI formation time. The role of the electrolyte salt was evidenced as the SECM maps clearly revealed insulating and homogeneous SEI-covered regions for the SEI formed in the presence of LiPF<sub>6</sub>, regardless of the chosen solvent (Figure 1D–E). Averaging the feedback current values at each SECM data point (pixel) and deriving the standard deviation at multiple points over the entire electrode surface is used as a measure of the homogeneity of the overall SEI-covered region (Figure 1I). Since the variation was below 30 % for all samples, it is reasonable to conclude that a homogeneous SEI is formed on Cu when a potential of 0 V is applied for 1 h, regardless of the electrolyte composition. This average value represents an averaged electronic insulating character which changes significantly with the electrolyte composition. The local properties of SEI obtained at different SEI formation cut-off potentials of +200 mV, +100 mV, and 0 mV (Figure 1F and G) were investigated with FB-SECM to elucidate its local heterogeneity. SEI formation with a cut-off potential of 200 mV led to a substantially higher heterogeneity of the electronic conductivity of the formed SEI. At a cut-off formation potential of 100 mV the SEI was more homogeneous, although the average feedback current value did not change significantly. Once a SEI was formed at a cut-off formation potential of 100 mV, further growth appears to be uniform and the average feedback current value decreases suggesting a more electronically insulating character of the formed SEI. This set of experiments shows the capability of the proposed

SECM methodology to provide averaged electronic conductivity information, with high data robustness due to averaging of the information from 100 to 250 individual FB-SECM measurements together with the local electronic conductivity data from the individual measurements.

To explore the complementarity of the proposed local FB-SECM measurements and global analysis, we were choosing graphite as current collector exhibiting a higher level of local heterogeneity. The global properties of the SEI formed on the entire graphite rod surface were investigated by means of voltammetry in presence of a free-diffusing redox couple (see section S-6 for more details).<sup>[29]</sup> It has to be pointed out that a Cu current collector was not feasible due to the Cu oxidation at the potential of the used redox mediator.<sup>[30]</sup> Additionally, using the proposed SECM methodology, the local electronic conductivity of the SEI on the graphite rod was elucidated. While the global cyclic voltammograms and EIS data showed a high blocking of the graphite surface for the charge transfer reaction of Fc oxidation after SEI (Figure S5), the corresponding SECM image (Figure 1H) identifies the presence of local defects in the freshly formed SEI. The average normalized FB-SECM currents over the different SEI are plotted in Figure 1I. Convincingly, it becomes obvious that despite the SEI formed on the graphite rod exhibits the expected highly electronically insulating character in average, the complementary local properties show a high level of heterogeneity, a result which could not have been anticipated from the global measurement.

SECM images revealed the presence of local heterogeneities which were masked in the global measurements. For a quantitative evaluation, the kinetics rate constants of the Fc oxidation reaction can be derived from FB-SECM approach curves. To this end, a series of FB-SECM approach curves were recorded in one direction ( $x$ - or  $y$ -) right after the FB-SECM image acquisition. Due to the comparatively long experimental time scale, we selected specific regions of interest in each FB-SECM image (top schemes in the Figure S4 in the Supporting Information) for more detailed and quantitative measurements of the electronic and ionic properties of the SEI-free and SEI-covered electrode surface. The selected regions crossed the SEI-free and uniformly SEI-covered areas. The sequence of FB-SECM approach curves was recorded by moving the tip first in the perpendicular direction ( $d$ , vertical direction) towards the surface, then retract it back to bulk, and finally move it in a lateral direction ( $x$ - or  $y$ -) to record subsequent approach curves at the next  $x$ - $y$ -location. All FB-SECM approach curves are shown as 2D-plot in Figure S4 (Supporting Information). The resulting approach curves were consistent with the expected behavior found in the FB-SECM images with a positive feedback response over the bare current collector surface and negative feedback above most of the SEI-covered regions confirming the insulating property of the SEI-covered regions.

Despite the electronic blockage and the prevention of a continuous cathodic degradation of the solvent the formed SEI and hence its importance for the long-term cycling stability of a LIB, it is of similar importance that the formed

SEI allows the permeation of desolvated Li-ions (Scheme 1B). We hypothesized that this ionic conductivity can be locally derived using multi-frequency AC-SECM at the same locations which were previously investigated using FB-SECM approach curves. AC-SECM was employed to acquire localized electrochemical impedance spectra as a function of local position over the precisely same region of the FB-SECM approach curves. The EIS measurements were recorded in the absence of the redox mediator Fc in the electrolyte at two working distances between tip and sample surface, specifically at a distance of 5  $\mu\text{m}$  and at 200  $\mu\text{m}$  sequentially for each  $x$ - or  $y$ -position. Two typical EIS spectra of the tip located in the bulk of the solution and close to the surface are shown in Figure 2. The sequences of EIS spectra recorded for each sample are summarized in section S-8 (Supporting Information). The EIS data obtained at a working distance of 5  $\mu\text{m}$  were strongly dependent on the lateral tip position and thus on the property of the sample surface. In other words, the EIS spectra were sensitive to the presence of the SEI on the Cu surface. Qualitatively, the results showed that the ionic charge transfer resistance increased for locations above the SEI (see EIS in Figure 2B and Figure S8 in the Supporting Information). For a quantitative assessment, the experimental data were fitted to an equivalent electric circuit (see Figure 2C and Figure 2D) to describe the tip response using a model of tip-sample surface interaction as described in the literature.<sup>[31]</sup> The local EIS data recorded close to the sample surface contain two contributions, i.e. the intrinsic tip contribution and the contribution due to the tip-to-sample interaction. Hence, the EIS spectra in the bulk electrolyte were used to deconvolute the contribution of the tip

contribution from the total response. Details about the used electronic equivalent circuit are described in the section S-8 (Supporting Information). After deconvoluting the tip contribution, the  $R_s$  and  $C_s$  elements were derived for each individual EIS spectrum recorded at each lateral position. The derived local ionic charge resistance element values ( $R_s$ ) are shown in the left-y axis of Figure 3 for each sample prepared with the parameters as summarized in Table 1.

The sequence of FB-SECM approach curves was plotted along with the lateral position ( $x$ - or  $y$ -) as a 3D plot in the same graphics of the AC-SECM parameters in Figure 3, resulting in an overlap of AC-SECM derived ionic resistance  $R_s$  (left  $y$ -axis) and a 3D plot of FB-SECM approach curves (background color scale). The individual approach curves were fitted to obtain the dimensionless parameter  $\kappa$ , which is derived from the first-order kinetic constant,  $k$ . The  $\kappa$  values represent the rate of the electron transfer reaction at the surface underneath the SECM tip. The  $\kappa$ -values are plotted on the right  $y$ -axis in Figure 3. The combination of the quantitative AC- and FB-SECM data is summarized in the Figure 3A and the resulting graph allows analyzing the local correlation between the properties of the SEI. In all independent analysis, the electron transfer kinetics and ionic charge transfer resistance over the free-SEI region were considered homogeneous.

Experimental parameters, such as the SEI formation protocol and the electrolyte composition, determine the properties of the SEI. To assess the role of each parameter on the SEI properties, we employed the correlative FB-SECM/AC-SECM over the same sample locations. The panels (B) and (C) (Figure 3) show the results for samples prepared with the long and short-term SEI formation protocols, respectively, in 1 M LiClO<sub>4</sub> and EC:PC formation. The FB-SECM data reveal the strong influence of the SEI-formation protocol on the electronic properties of the resulting SEI in this electrolyte. The long-term SEI-formation exhibits substantial benefits for inhibiting electron transfer across the SEI. The results also revealed some heterogeneity of the insulating SEI (at  $X=300 \mu\text{m}$ ), likely caused by substrate heterogeneities but in this case presumably due to the effects of the O-ring sealing the electrochemical cell during in the long-term SEI formation. These O-ring induced heterogeneities on smooth Cu electrodes simulate potential heterogeneities in more complex electrodes, e.g. graphite (edges versus basal planes) or Si (volumetric changes inducing cracks in the SEI). It should be noted that the smaller working distance in AC-SECM (5  $\mu\text{m}$ ) prevents the detection of small defects since the tip should be positioned precisely over the defect spot. In any case, the ionic charge transfer resistance over the SEI was significantly higher for the long-term SEI formation than for the short-term SEI-formation.

The nature of the Li salt used as the electrolyte is expected to play an essential role not only in the composition but also in the properties of the SEI. Hence, the SEI formed in 1 M LiPF<sub>6</sub> in EC:PC (50/50 wt %) solution was analyzed and compared with that formed using LiClO<sub>4</sub>. Results obtained for 1 M LiPF<sub>6</sub> in EC:PC are displayed in panels D in Figure 3. If the SEI was created in 1 M LiPF<sub>6</sub> in

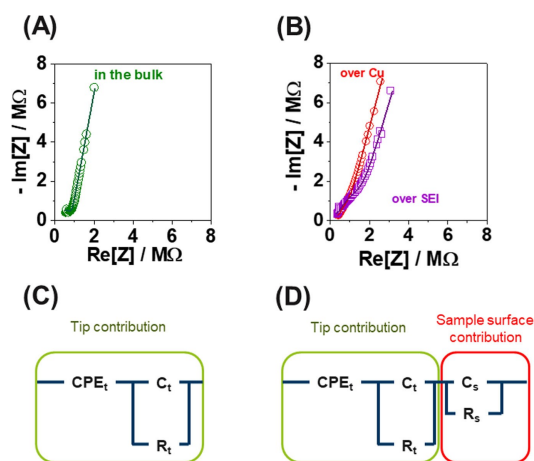


**Figure 2.** Nyquist plot of typical EIS data obtained using a Pt microelectrode (diameter: 25  $\mu\text{m}$ ) in 1 mM LiClO<sub>4</sub> EC:PC (50/50 wt%) as electrolyte solution when the tip was positioned A) in the bulk of solution and B) at a working distance of 5  $\mu\text{m}$  from the sample surface (red and circles over the copper, and purple and squares over the SEI). Scatter plot: experimental data. Straight line: fitting results. DC potential: OCP. AC bias: 10 mV (rms).  $f$ : 50 kHz to 500 Hz. C) and D) Electric equivalent circuits used for the mathematical fits to describe the local impedance response of the tip, where  $CPE_t$ ,  $C_t$  and  $R_t$  are elements associated with the tip contribution, and the  $R_s$  and  $C_s$  are correlated with the sample surface.

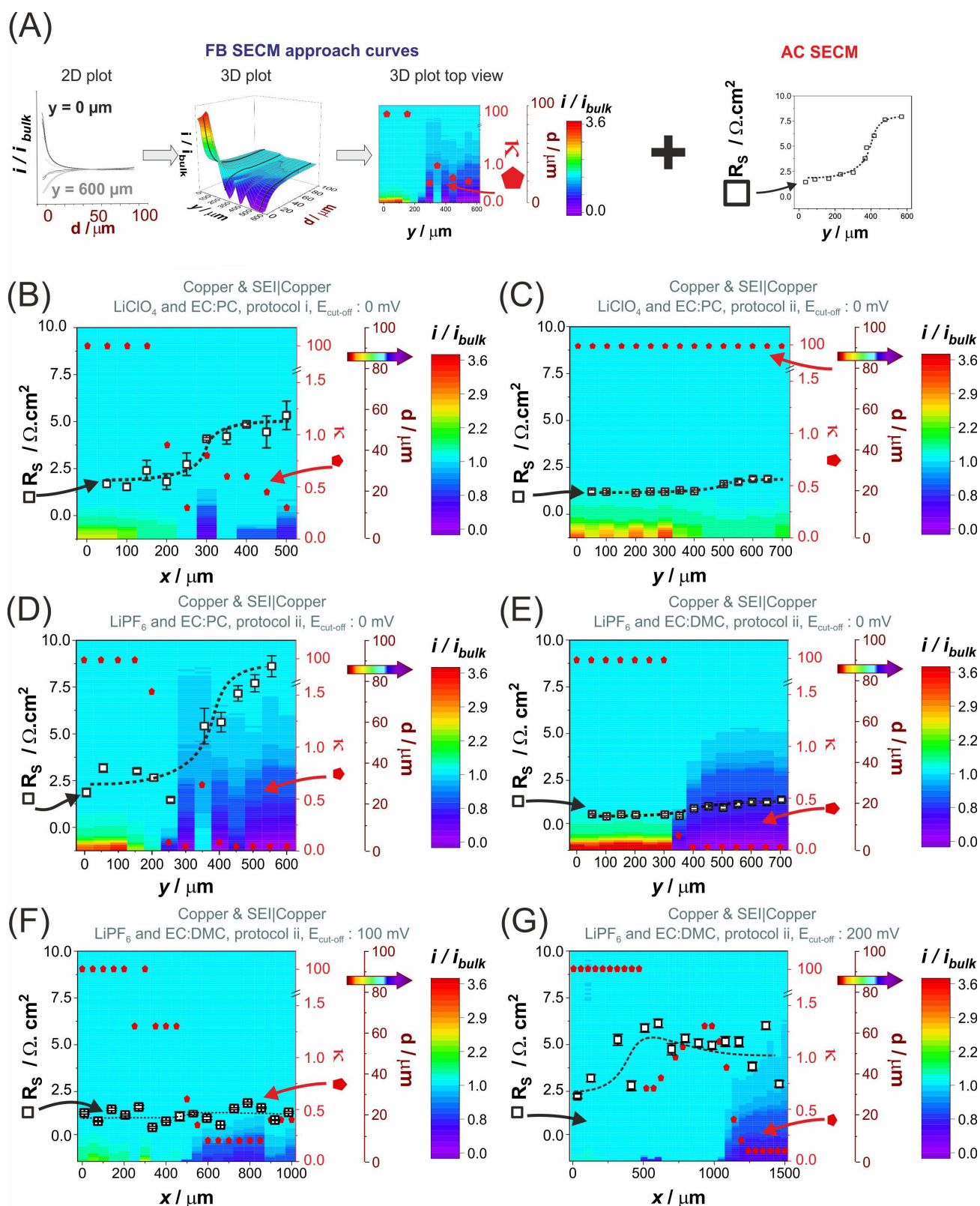


**Figure 3.** FB-SECM and AC-SECM measurements at the interrogated area covering the SEI-free (left) and SEI-covered (right) regions. The SEI formation parameters are specified in Table 1. A) Scheme of the combination of 3D-plot FB-SECM approach curves and AC SECM values graphics. B)–G) Left y-axis: calculated  $R_s$  values distribution obtained by local EIS measurements at a working distance of  $5 \mu\text{m}$  in the multi-frequency AC-SECM measurements. B)–G) Right y-axis:  $\kappa$  = dimensionless parameter of the first order kinetic electron transfer rate constant,  $k$  ( $\text{m s}^{-1}$ ), calculated fit for each approach curve. B)–G) Right y-axis: vertical/perpendicular distance of the 3D-plot of the FB approach curves,  $d$ , in function of lateral distance ( $x$ - or  $y$ -). B)–G) Colored background scale: normalized current map in the 3D-plot of the sequence of approach curves as a function of the lateral position, with a perpendicular increment of  $1 \mu\text{m}$  and a lateral increment of  $50 \mu\text{m}$ .  $E_{\text{tip}}: 3.5 \text{ V vs. RE}$ .

EC:PC and short-term SEI formation protocol, a high contrast and well-defined boundary between SEI-free and SEI-covered regions are visible, which reveals the importance of the presence of LiPF<sub>6</sub> in the formation of an effectively protecting SEI against electron transfer reactions ( $\kappa$  values < 1). However, the ionic charge transfer resistance was also higher than that obtained for SEIs formed in the presence of LiClO<sub>4</sub>. This is an undesired feature since higher ionic resistance would lead to higher internal resistance during battery operation, which demonstrates the importance to reveal simultaneously the electron and ion charge transfer properties of an SEI.

The solvent or solvent composition is another factor in the SEI formation. Hence, we formed SEI on Cu in an electrolyte solution in which PC was replaced by DMC. The results for the SEI formed using the short-term protocol in 1 M LiPF<sub>6</sub> and EC:DMC 50/50 (v/v) electrolyte are presented in panels E of Figure 3. The FB-SECM data show a high homogeneity of the hindered electron transfer over the SEI-covered region ( $\kappa < 1$ ). Furthermore, high uniformity in the SEI-free area and the boundary between the two regions was observed. SECM measurements consist of multiple local independent analysis and hence reveal the heterogeneity at the micro-scale. For the ionic charge transfer resistance calculated from the AC-SECM results, the replacement of PC by DMC led to drastic changes. The ionic charge transfer resistance over the SEI-covered region was substantially decreased, which makes 1 M LiPF<sub>6</sub> and EC:DMC the best electrolyte composition studied here due to the effective hindrance of electron transfer and relatively low ionic charge transfer resistance. Additionally, results of the SEI formed using 1 M LiPF<sub>6</sub> and EC:DMC as electrolyte at different formation cut-off potentials (+200 mV, 100 mV and 0 mV) revealed heterogeneous SEI growth. The  $\kappa$  values indicated an electronically insulating character of the SEI. Results in Figure 3 and Figure 11 indicate that an electronically insulating SEI with significant heterogeneity is formed at a cut-off formation potential of +200 mV. At a cut-off formation potential +100 mV the SEI became more homogeneous, however, its electronically insulating character did not change significantly. Polarization to the cut-off formation potential of 0 mV led to an increase in the electronically insulating character while maintaining homogeneity. In short, the results in Figure 3 provide the basis for the three main conclusions: i) long SEI formation protocols lead to improved protecting properties (electronically insulating character). ii) LiPF<sub>6</sub> is of key importance to promote the formation of a protecting SEI (electronically insulating). iii) The substitution of PC by a linear co-solvent such as DMC is beneficial for reducing the charge transfer resistance (ionically conducting SEI). These results correlate with results from literature: i) in practice, very slow and time-consuming first charging cycles are carried out by the manufactures to improve the effectiveness of the SEI.<sup>[32]</sup> ii) LiF originating from the use of LiPF<sub>6</sub> is considered a key element in the SEI.<sup>[33]</sup> Grey et al. recently confirmed<sup>[34]</sup> that a native SEI rich in LiF is spontaneously formed which correlates with the high electronically insulating character found when using LiPF<sub>6</sub>. iii) Using a model Li<sub>4</sub>Ti<sub>5</sub>O<sub>12</sub> electrode, Abe et al.<sup>[35]</sup> were able to study the influence of the electrolyte co-solvent on the charge transfer resistance demon-

strating that the use of PC leads to higher ionic resistance. We provide a proof of concept demonstrating that the proposed methodology is capable to describing quantitatively and laterally-resolved the ionic and electronic properties of differently formed SEI. In addition, the EIS data provide local values of the double layer capacitance (Figure S10 in Supporting Information). In general, all samples followed the same trend: a clear change in  $C_s$  over the boundary of the two regions was observed, with the  $C_s$  values dropping when crossing from the SEI-free to the SEI-covered region. Interestingly, the bare electrode surface showed higher  $C_s$  values than those obtained over the SEI-covered region, which is attributed to the presence of oxides from the native thin surface film of CuO. To further demonstrate the sensitivity of our proposed methodology,  $C_s$  values were calculated for a sample using glassy carbon as the current collector. The  $C_s$  values over the SEI-free and SEI-covered regions were very similar in the case of glassy carbon. The  $C_s$  values over the SEI-covered region were about 40 pC, which is similar to the values obtained over the SEI-covered Cu current collector. Indeed, the changes attributed to the SEI-free regions are due to the properties of the different current collectors.

Moreover, the local  $R_s$  and  $C_s$  are correlated to the intrinsic values of the dielectric permittivity ( $\epsilon$ ) and resistivity ( $\rho$ ), respectively. As the determination of the SEI thickness was not possible due to the roughness of the current collector, exact values of  $\epsilon$  and the  $\rho$  cannot be provided. Instead, an average value of the SEI can be assumed, i.e. 50 nm, so that approximate values can be estimated (section S-11 of the Supporting Information), which will at least provide the order of magnitude of these parameters. Quantitative information may be possible by precise determination of the SEI thickness e.g. by using techniques such as dilatometry<sup>[36]</sup> AFM-nanoindentation<sup>[37]</sup> and neutron reflectometry.<sup>[38]</sup>

## Conclusion

A methodology based on a sequential combination of correlative FB- and AC-SECM measurements inside an Ar-filled glovebox was established, which provides in situ and local quantitative information of the electronic and ionic properties of the SEI for the first time. The feasibility of the spatially resolved methodology was demonstrated by investigating the influence of the electrolyte composition on the properties of the resulting SEI, concluding that both electrolyte salt and solvent play a significant role in their impact on both electronic and ionic properties of the formed SEI, as expected but demonstrated here for the first time. Regarding the ionic properties, the intrinsic dielectric permittivity and ionic resistivity of the SEI can be determined, provided that the thickness of the layer is known. Thus, the proposed methodology is able to provide in situ and spatially resolved information of the two most important properties of the SEI. Considering that the SEI is a core topic in Li-ion batteries due to its indisputable importance on battery performances, the examples discussed in this work show that variations in electrolyte composition lead to enormous changes in the

electronic and ionic conductivities, and anticipate the impact of the technique in Li-ion battery research.

### Acknowledgements

The authors are grateful for financial support by the European Union's Horizon 2020 research and innovation programme under grant agreement NanoBat No 861962 as well as to the Deutsche Forschungsgemeinschaft ((DFG, German Research Foundation) under Germany's Excellence Strategy—EXC 2033-390677874—RESOLV. The authors thank Martin Trautmann for the AFM measurements. Open Access funding enabled and organized by Projekt DEAL.

### Conflict of Interest

The authors declare no conflict of interest.

### Data Availability Statement

The data that support the findings of this study are available from the corresponding author upon reasonable request.

**Keywords:** Li-Ion Batteries · Local Electrochemical Impedance Spectroscopy · SEI Properties · Scanning Electrochemical Microscopy · Solid Electrolyte Interphase

- [1] D. Liu, Z. Shadike, R. Lin, K. Qian, H. Li, K. Li, S. Wang, Q. Yu, M. Liu, S. Ganapathy, X. Qin, Q.-H. Yang, M. Wage-maker, F. Kang, X.-Q. Yang, B. Li, *Adv. Mater.* **2019**, *31*, 1806620.
- [2] a) M. G. Boebinger, J. A. Lewis, S. E. Sandoval, M. T. McDowell, *ACS Energy Lett.* **2020**, *5*, 335; b) J.-H. Tian, T. Jiang, M. Wang, Z. Hu, X. Zhu, L. Zhang, T. Qian, C. Yan, *Small Methods* **2020**, *4*, 1900467.
- [3] a) J. R. Rodriguez, S. B. Aguirre, V. G. Pol, *J. Power Sources* **2019**, *437*, 226851; b) X.-C. Ren, X.-Q. Zhang, R. Xu, J.-Q. Huang, Q. Zhang, *Adv. Mater.* **2020**, *32*, 1908293.
- [4] R. Kempaiah, G. Vasudevamurthy, A. Subramanian, *Nano Energy* **2019**, *65*, 103925.
- [5] M. Gauthier, T. J. Carney, A. Grimaud, L. Giordano, N. Pour, H.-H. Chang, D. P. Fenning, S. F. Lux, O. Paschos, C. Bauer, F. Maglia, S. Lupart, P. Lamp, Y. Shao-Horn, *J. Phys. Chem. Lett.* **2015**, *6*, 4653.
- [6] S. Daboss, F. Rahmanian, H. S. Stein, C. Kranz, *Elec. Sci. Adv.* **2021**, e2100122.
- [7] a) L. Danis, S. M. Gateman, C. Kuss, S. B. Schougaard, J. Mauzeroll, *ChemElectroChem* **2017**, *4*, 6; b) E. Ventosa, *Curr. Opin. Electrochem.* **2021**, *25*, 100635.
- [8] A. Kumatani, T. Matsue, *Curr. Opin. Electrochem.* **2020**, *22*, 228.
- [9] a) F. Xu, B. Beak, C. Jung, *J. Solid State Electrochem.* **2012**, *16*, 305; b) M. S. Hossain, L. I. Stephens, M. Hatami, M. Ghavidel, D. Chhin, J. I. G. Dawkins, L. Savignac, J. Mauzeroll, S. B. Schougaard, *ACS Appl. Energy Mater.* **2020**, *3*, 440.
- [10] G. Zampardi, E. Ventosa, F. La Mantia, W. Schuhmann, *Chem. Commun.* **2013**, *49*, 9347.
- [11] H. Bülter, F. Peters, J. Schwenzel, G. Wittstock, *Angew. Chem. Int. Ed.* **2014**, *53*, 10531; *Angew. Chem.* **2014**, *126*, 10699.
- [12] E. Ventosa, W. Schuhmann, *Phys. Chem. Chem. Phys.* **2015**, *17*, 28441.
- [13] E. Ventosa, E. Madej, G. Zampardi, B. Mei, P. Weide, H. Antoni, F. La Mantia, M. Muhler, W. Schuhmann, *ACS Appl. Mater. Interfaces* **2017**, *9*, 3123.
- [14] T. Löffler, J. Clausmeyer, P. Wilde, K. Tschulik, W. Schuhmann, E. Ventosa, *Nano Energy* **2019**, *57*, 827.
- [15] B. Krueger, L. Balboa, J. F. Dohmann, M. Winter, P. Bieker, G. Wittstock, *ChemElectroChem* **2020**, *7*, 3590.
- [16] M. Winter, *Z. Phys. Chem.* **2009**, *223*, 1395.
- [17] a) B. R. Horrocks, D. Schmidtke, A. Heller, A. J. Bard, *Anal. Chem.* **1993**, *65*, 3605; b) M. A. Alpuche-Aviles, D. O. Wipf, *Anal. Chem.* **2001**, *73*, 4873; c) B. Ballesteros Katemann, *Electrochem. Commun.* **2002**, *4*, 134.
- [18] D. Liu, X. Zeng, S. Liu, S. Wang, F. Kang, B. Li, *ChemElectroChem* **2019**, *6*, 4854.
- [19] A. Baranski, P. Diakowski, *J. Solid State Electrochem.* **2004**, *8*, 683.
- [20] A. Schulte, S. Belger, M. Etienne, W. Schuhmann, *Mater. Sci. Eng. A* **2004**, *378*, 523.
- [21] K. Eckhard, W. Schuhmann, *Analyst* **2008**, *133*, 1486.
- [22] K. Eckhard, T. Erichsen, M. Stratmann, W. Schuhmann, *Chem. Eur. J.* **2008**, *14*, 3968.
- [23] D. Liu, Q. Yu, S. Liu, K. Qian, S. Wang, W. Sun, X.-Q. Yang, F. Kang, B. Li, *J. Phys. Chem. C* **2019**, *123*, 12797.
- [24] J. Kwak, A. J. Bard, *Anal. Chem.* **1989**, *61*, 1221.
- [25] A. J. Bard, F. R. F. Fan, J. Kwak, O. Lev, *Anal. Chem.* **1989**, *61*, 132.
- [26] H. Bülter, P. Schwager, D. Fenske, G. Wittstock, *Electrochim. Acta* **2016**, *199*, 366.
- [27] E. dos Santos Sardinha, M. Sternad, H. M. R. Wilkening, G. Wittstock, *ACS Appl. Energy Mater.* **2019**, *2*, 1388.
- [28] X.-B. Cheng, R. Zhang, C.-Z. Zhao, F. Wei, J.-G. Zhang, Q. Zhang, *Adv. Sci.* **2016**, *3*, 1500213.
- [29] C. O. Laoire, E. Plichta, M. Hendrickson, S. Mukerjee, K. M. Abraham, *Electrochim. Acta* **2009**, *54*, 6560.
- [30] M. Zhao, S. Kariuki, H. D. Dewald, F. R. Lemke, R. J. Staniewicz, E. J. Plichta, R. A. Marsh, *J. Electrochem. Soc.* **2000**, *147*, 2874.
- [31] A. S. Bandarenka, A. Maljusch, V. Kuznetsov, K. Eckhard, W. Schuhmann, *J. Phys. Chem. C* **2014**, *118*, 8952.
- [32] Y. Liu, R. Zhang, J. Wang, Y. Wang, *iScience* **2021**, *24*, 102332.
- [33] J. Tan, J. Matz, P. Dong, J. Shen, M. Ye, *Adv. Energy Mater.* **2021**, *11*, 2100046.
- [34] S. Menkin, C. A. O'Keefe, A. B. Gunnarsdóttir, S. Dey, F. M. Pesci, Z. Shen, A. Aguadero, C. P. Grey, *J. Phys. Chem. C* **2021**, *125*, 16719.
- [35] R. N. Nasara, W. Ma, Y. Kondo, K. Miyazaki, Y. Miyahara, T. Fukutsuka, C.-A. Lin, S.-K. Lin, T. Abe, *ChemSusChem* **2020**, *13*, 4041.
- [36] H. Michael, R. Jervis, D. J. L. Brett, P. R. Shearing, *Batteries Supercaps* **2021**, *4*, 1378.
- [37] V. Kuznetsov, A.-H. Zinn, G. Zampardi, S. Borhani-Haghighi, F. La Mantia, A. Ludwig, W. Schuhmann, E. Ventosa, *ACS Appl. Mater. Interfaces* **2015**, *7*, 23554.
- [38] G. M. Veith, M. Doucet, J. K. Baldwin, R. L. Sacci, T. M. Fears, Y. Wang, J. F. Browning, *J. Phys. Chem. C* **2015**, *119*, 20339.

Manuscript received: February 19, 2022

Accepted manuscript online: March 21, 2022

Version of record online: May 5, 2022